ASME Journal of Applied Mechanics
Online journal at:
https://asmedigitalcollection.asme.org/appliedmechanics

Ahmad Almamo
State Key Laboratory of CAD & CG,
Key Laboratory of Soft Machines and
Smart Devices of Zhejiang Province,
Soft Matter Research Center,
Department of Engineering Mechanics,
Zhejiang University,
Hangzhou 310027, China
e-mail: ahmadalmamo@zju.edu.cn

Yipin Su[1]
State Key Laboratory of CAD & CG,
Key Laboratory of Soft Machines and
Smart Devices of Zhejiang Province,
Soft Matter Research Center,
Department of Engineering Mechanics,
Zhejiang University,
Hangzhou 310027, China;
Qihang Union & Innovation Center,
Huanjiang Laboratory,
Zhuji 311800, China
e-mail: su_yp@zju.edu.cn

Weiqiu Chen
State Key Laboratory of CAD & CG,
Key Laboratory of Soft Machines and
Smart Devices of Zhejiang Province,
Soft Matter Research Center,
Department of Engineering Mechanics,
Zhejiang University,
Hangzhou 310027, China;
Center for Soft Machines and Smart Devices,
Huanjiang Laboratory,
Zhuji 311800, China;
Faculty of Mechanical Engineering and
Mechanics,
Ningbo University,
Ningbo 315211, China
e-mail: chenwq@zju.edu.cn

Huiming Wang
State Key Laboratory of CAD & CG,
Key Laboratory of Soft Machines and
Smart Devices of Zhejiang Province,
Soft Matter Research Center,
Department of Engineering Mechanics,
Zhejiang University,
Hangzhou 310027, China
e-mail: wanghuiming@zju.edu.cn

Axisymmetric Vibration of Inviscid Compressible Fluid-Filled Soft Dielectric Elastomer Actuator Tube

Driven by the versatility and adaptability of next-generation soft robotic devices, investigating the vibrational behavior under fluid-electromechanical coupling represented by a soft dielectric elastomer actuator (DEA) tube filled with fluid evokes much attention. Here, we investigate the axisymmetric vibration of an inviscid compressible fluid-filled thin DEA tube by using the Gent model to define the behavior of the tube under multi-fields. We consider the effect of the fluid by exploiting the relation of the radial fluid pressure at the fluid–solid interface. Following the general incremental theory of nonlinear electro-elasticity, we formulate the incremental governing and constitutive equations needed for vibration analysis and solve them numerically using the state-space method (SSM). The results demonstrate the influence of the applied voltage, overcritical circumferential stretch, higher frequency modes, and phase velocity modes on the early development of axisymmetric instability and dielectric breakdown. The existence of the fluid contributes to more reduction in the frequency and phase velocity compared to the fluid-free case due to the added mass effect. Moreover, the results show the role of fluid in the partial self-healing of the soft DEA. A parametric study on specific variables deduces that increasing the thickness of the soft DEA tube reduces the frequency effectively, whereas applying higher voltages causes a thinning in the thickness, leading to the need for thicker tubes.
[DOI: 10.1115/1.4065794]

Keywords: constitutive modeling of materials, elasticity, structures, vibration

1 Introduction

Many analytical models have been utilized as a keystone to describe wave propagation in elastic tubes for some biological applications, including blood flow in arteries and electromechanical

[1]Corresponding author.

Contributed by the Applied Mechanics Division of ASME for publication in the Journal of Applied Mechanics. Manuscript received January 14, 2024; final manuscript received April 2, 2024; published online July 12, 2024. Assoc. Editor: Yuhang Hu.

cardiovascular activity, as seen in the study by Bathe and Kamm [1]. Soft dielectric elastomer actuators (DEAs) inspired numerous applications, particularly artificial muscles and other biomedical devices [2–6].

Soft DEAs have garnered significant attention from scientists due to their unique properties, particularly their behavior under multiphysics. Among these, fluid-filled soft actuators have gained traction due to their merits over classical soft actuators. They improve efficiency, performance, response speed, and portability, while the current soft actuators, such as pneumatics or shape-memory alloys, suffer some limitations [7–9]. The fluid-filled soft DEAs demonstrate controllable linear contraction, higher bandwidth, and actuation at high frequency, making them suitable for applications in bioinspired robotics, active prostheses, medical and industrial automation, autonomous soft robotic devices, and gripping systems [7,8,10–15]. The filled compressed fluid allows the soft DEAs to self-heal after electric breakdown, which the conventional DEAs cannot achieve [8–10,16].

The tubular dielectric actuators, early introduced by Pelrine et al. [17] and under the effects of biasing fields, were considered by Baumhauer and Tiersten [18] for small-amplitude wave propagation in electro-elastic materials. Alongside, the general nonlinear theory of electro-elasticity, established by Toupin [19,20] for the static and dynamics problems, drove to improve theoretical models to simulate and confirm the obtained experimental results for DEAs [21–23]. The axisymmetric wave propagation of soft tubular DEAs was also investigated to illustrate the effect of radial biasing fields [24,25]. It has been found that the higher applied voltage leads to large deformation in a soft dielectric tube and causes instabilities once the voltage approaches the critical value [26–28].

Axisymmetric wave propagation in the coupled fluid–solid system was early examined by Biot [29] to find the phase and group velocities in a cylindrical bore through an elastic material of infinite extent filled with fluid. Meanwhile, Fuller and Fahy [30] investigated free wave dispersion behavior and energy distributions in a fluid-filled, thin-walled cylindrical elastic shell. Beyond DEAs, many studies have been carried out to analyze the wave propagation through functionally graded piezoelectric materials either immersed in fluid as in the study by Chen and Bian [31] or filled with the fluid as shown by Chen et al. [32].

Recently, the effect of an electric field on the axisymmetric solitary wave in a fluid-filled, thin-walled dielectric elastomer (DE) tube was studied by Defaz et al. [33]. Furthermore, the axisymmetric vibration of multilayered electroactive circular plates in contact with fluid was examined by Cao et al. [34]. Although Rothemund et al. [11] presented a model to analyze the dynamic behavior of electrohydraulic soft actuators by examining in detail the influence of geometry, materials system, and external loads on the actuation speed, they did not consider optimizing the performance of soft DEAs by investigating the effect of some parameters, such as the densities and elastic wave velocities in the fluid and DEAs. Thus, vibration and wave propagation in the coupled fluid-DEA system still have many research gaps worthy of interest. Accordingly, by our work, we conduct an axisymmetric vibration analysis of the fluid-filled thin-walled DEA tube using the proper mathematical technique, namely, the state-space method (SSM), to solve the system of ordinary differential equations representing the incremental governing equations within the numerical context. Furthermore, we study the effect of some physical quantities and explain how they affect the vibrational behavior of DEAs.

The arrangement of this article has the following style. In Sec. 2, we explain the basic equations, including the governing and constitutive equations, required for formulating our problem. The linearized incremental analysis, comprising the incremental governing and constitutive equations besides the incremental boundary conditions, is detailed in Sec. 3. The mathematical model of the energy function describing the material behavior according to the finite deformation and assumed constraints is demonstrated in Sec. 4. The SSM required for solving the system of incremental equations of motion is also explained in this section. The obtained numerical results are visualized and discussed in Sec. 5. In Sec. 6, we draw conclusions based on the observed results and the main findings of our work.

2 Theoretical Background

Let us consider an isotropic incompressible soft DEA tube with inner and outer radii (R_i, R_o) and initial length L as depicted in Fig. 1. The tube is filled with a compressible inviscid fluid and subject to extension and inflation induced by pressure applied at the outer surface P_o. A voltage V is applied through the soft DEA tube's thickness, where the inner and outer surfaces are coated with flexible electrodes.

2.1 Axisymmetric Deformation and Electric Field.

In the referential cylindrical system (R, Θ, Z), a material particle in the undeformed configuration is defined by its position vector $\boldsymbol{X}(R, \Theta, Z)$. In contrast, the material particle $\boldsymbol{X}$ has the position $\boldsymbol{x}(r, \theta, z)$ in the deformed configuration and current cylindrical system (r, θ, z).

In Fig. 1, $H = R_o - R_i$ represents the thickness of the soft DEA tube. The counterpart geometric parameters of R_i, R_o, L, and H in the deformed configuration are r_i, r_o, l, and $h = r_o - r_i$.

In the undeformed configuration, the Lagrangian geometries of the tube in the cylindrical coordinates (R, Θ, Z) for the position of an arbitrary point read

$$0 < R_i \le R \le R_o, \quad 0 \le \Theta \le 2\pi, \quad -L/2 \le Z \le L/2 \tag{1}$$

After deformation, we obtain the Eulerian geometries in the updated cylindrical coordinates (r, θ, z)

$$0 < r_i \le r \le r_o, \quad 0 \le \theta \le 2\pi, \quad -l/2 \le z \le l/2 \tag{2}$$

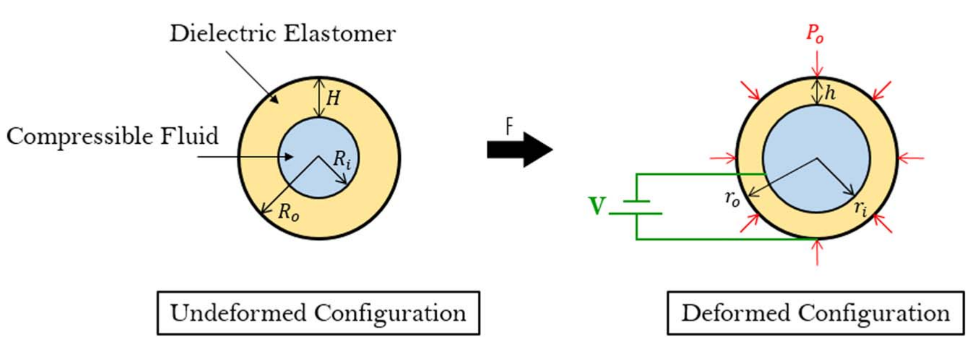

Fig. 1 Illustrative sketch of a soft DEA tube filled with an inviscid compressible fluid

The deformation gradient tensor $\boldsymbol{F} = \partial \boldsymbol{x}/\partial \boldsymbol{X}$ reads

$$\boldsymbol{F} = \begin{bmatrix} \dfrac{\partial r}{\partial R} & \dfrac{\partial r}{R\partial \Theta} & \dfrac{\partial r}{\partial Z} \\ \dfrac{r\partial \theta}{\partial R} & \dfrac{r\partial \theta}{R\partial \Theta} & \dfrac{r\partial \theta}{\partial Z} \\ \dfrac{\partial z}{\partial R} & \dfrac{\partial z}{R\partial \Theta} & \dfrac{\partial z}{\partial Z} \end{bmatrix} = \begin{bmatrix} \lambda_r & 0 & 0 \\ 0 & \lambda & 0 \\ 0 & 0 & \lambda_z \end{bmatrix} \tag{3}$$

$$\begin{aligned} I_1 &= \mathrm{tr}\,\boldsymbol{C} = \lambda_r^2 + \lambda^2 + \lambda_z^2, \\ I_2 &= \mathrm{tr}(\boldsymbol{C}^{-1}) = \lambda_r^{-2} + \lambda^{-2} + \lambda_z^{-2}, \quad I_3 = 1 \end{aligned} \tag{4}$$

$\lambda_r = \lambda^{-1}\lambda_z^{-1}$ and I_1, I_2, I_3 are the first three principal scalar invariants. It should be noted that the incompressibility condition has been used; therefore, $I_3 = 1$. $\boldsymbol{C} = \boldsymbol{F}^{\mathrm{T}}\boldsymbol{F}$ is the right Cauchy–Green deformation tensor, and $\lambda = r/R$ is the circumferential stretch of the material.

$(\cdot)^{\mathrm{T}}$ and $(\cdot)^{-1}$, here and after, refer to the transpose and inverse of a tensor, respectively. For incompressible materials, the axisymmetric deformation of the soft DEA tube is

$$\lambda_z(r^2 - r_i^2) = R^2 - R_i^2, \quad \theta = \Theta, \quad \lambda_z = \frac{z}{Z} = \frac{l}{L} \tag{5}$$

where λ_z is the axial stretch. By Eq. (5), and for a given $\lambda_i = r_i/R_i$ at the inner surface, the circumferential stretches of the outer surfaces λ_o are

$$\lambda_o = r_o/R_o = \sqrt{\lambda_i^2 \cdot \eta^2 + \lambda_z^{-1}(1 - \eta^2)} \tag{6}$$

where $\eta = R_i/R_o$ is the aspect ratio of the soft DEA tube.

To consider an axisymmetric plane strain problem, we fix the coordinates $\theta = \Theta$ and take the length of the tube much greater than the thickness of the dielectric layer ($L \gg H$). The actual electric field $\boldsymbol{E}$ and electric displacement $\boldsymbol{D}$ in the soft DEA tube generated by the potential difference applied between the electrodes at the inner and outer surfaces are

$$\boldsymbol{E} = \begin{bmatrix} E_r & 0 & 0 \end{bmatrix}^{\mathrm{T}}, \quad \boldsymbol{D} = \begin{bmatrix} D_r & 0 & 0 \end{bmatrix}^{\mathrm{T}} \tag{7}$$

where E_r and D_r are the radial components of the actual electric field and electric displacement, respectively. For an ideal DEA tube, the actual radial electric field can be obtained [35]

$$E_r = \varepsilon^{-1} D_r = \frac{V}{r}\left(\ln \frac{r_o}{r_i}\right)^{-1} \tag{8}$$

where ε is the permittivity of the material. The electric field outside the DEA tube is assumed to be a vacuum so that it can be ignored.

2.2 Constitutive Equations and Boundary Conditions.

The energy function of the ideal DEA tube Σ can be described as follows [36]:

$$\Sigma = W(I_1) + \frac{1}{2}\varepsilon^{-1} I_5 \tag{9}$$

where W is the elastic part of the energy function and $I_5 = D_r^2$. Thus, the total Cauchy stress and actual electric field are [37]

$$\boldsymbol{\tau} = 2W_1\boldsymbol{B} - p\mathbf{I} + \varepsilon^{-1}\boldsymbol{D} \otimes \boldsymbol{D}, \quad \boldsymbol{E} = \varepsilon^{-1}\boldsymbol{D} \tag{10}$$

where $W_1 = \partial W/\partial I_1$, $\boldsymbol{B} = \boldsymbol{F}\boldsymbol{F}^{\mathrm{T}}$ is the left Cauchy–Green deformation tensor, and $\mathbf{I}$ is the identity tensor. p is a Lagrange multiplier, which can be determined from the boundary conditions.

The stress components of the DEA tube can be expressed as follows [38]:

$$\begin{aligned} &\tau_{rr} = 2W_1\lambda_r^2 - p + \varepsilon^{-1}D_r^2, \quad \tau_{\theta\theta} = 2W_1\lambda^2 - p, \\ &\tau_{zz} = 2W_1\lambda_z^2 - p \end{aligned} \tag{11}$$

Then, the equilibrium equation of the tube can be written as follows:

$$\frac{d\tau_{rr}}{dr} + \frac{\tau_{rr} - \tau_{\theta\theta}}{r} = 0 \tag{12}$$

and the corresponding boundary conditions at both ends $z = \pm l/2$ and inner and outer surfaces are as follows:

$$\tau_{rr}(r_i) = -P_f, \quad \tau_{rr}(r_o) = -P_o, \quad \tau_{rz}(\pm l/2) = 0 \tag{13}$$

where $P_f = \omega^2 B(r_i)\rho_f$ is the dynamic fluid pressure, ω is the circular frequency, and ρ_f is the fluid density. P_o represents the applied external pressure. $B(r)$ is the coupling function between the compressible fluid and the tube [39]. Then, $B(r_o) = 0$, and at the contact to the fluid surface [32]

$$B(r_i) = \begin{cases} \dfrac{J_n(\chi)}{J_{n-1}(\chi) - J_{n+1}(\chi)} \cdot \dfrac{2}{\chi}, & \chi^2 > 0 \\ \dfrac{1}{n}, & \chi^2 = 0 \\ \dfrac{I_n(\tilde{\chi})}{I_{n-1}(\tilde{\chi}) + I_{n+1}(\tilde{\chi})} \cdot \dfrac{2}{\tilde{\chi}}, & \chi^2 = -\tilde{\chi}^2 < 0 \end{cases} \tag{14}$$

where $J_n(\chi)$ and $I_n(\chi)$ are the Bessel function and the modified Bessel function of the first kind, respectively. $\chi^2 = (\omega^2/c_f^2) - \alpha^2$ is the internal fluid radial wavenumber, where c_f is the elastic wave velocity in fluid, $\alpha = 2n\pi/l$ designates the axial wavenumber, whereas $n = 1, 2, 3, \ldots$ represents the axial mode number.

A variety of properties of a system can be analyzed using the applied pressure expression in conjunction with the characteristics equation as given below:

$$\begin{aligned} \Delta P = P_i - P_o &= \int_{r_i}^{r_o} \frac{d\tau_{rr}}{dr}\,dr = \int_{r_i}^{r_o} 2W_1(\lambda^2 - \lambda_r^2)\frac{dr}{r} \\ &\quad - \frac{V^2}{2r_i^2(\ln(r_o/r_i))^2}\left(1 - \frac{r_i^2}{r_o^2}\right) + P_f \end{aligned} \tag{15}$$

where the inner pressure $P_i = P_f$. For known P_f and λ_i, τ_{rr} reads [40]

$$\tau_{rr} = P_f + \int_{\lambda_i}^{r/R} \frac{2W_1(\lambda^2 - \lambda_r^2)}{\lambda - \lambda_z\lambda^3}\,d\lambda - \frac{V^2}{2r_i^2(\ln(r_a/r_i))^2}\left(1 - \frac{r_i^2}{r^2}\right) \tag{16}$$

and from Eq. $(11)_1$, p is

$$\begin{aligned} p = 2W_1\lambda_r^2 - P_f - \int_{\lambda_i}^{r/R} \frac{2W_1(\lambda^2 - \lambda_r^2)}{\lambda - \lambda_z\lambda^3}\,d\lambda \\ + \frac{V^2}{2r_i^2(\ln(r_\sigma/r_i))^2}\left(1 - \frac{r_i^2}{r^2}\right) + \varepsilon^{-1}D_r^2 \end{aligned} \tag{17}$$

3 Linearized Incremental Analysis

3.1 Incremental Constitutive Equations.

Due to the deformed configuration, we superimpose a time-dependent incremental displacement $\boldsymbol{u}$, along with an incremental electric displacement $\dot{\boldsymbol{D}}$ in the updated Eulerian form. $(\dot{\cdot})$ indicates an incremental quantity from here onwards.

The incremental total nominal stress $\dot{\boldsymbol{T}}$ and incremental electric field $\dot{\boldsymbol{E}}$ in the updated Eulerian form have the relations [41]

$$\dot{\boldsymbol{T}} = \boldsymbol{A}\boldsymbol{L} + \boldsymbol{\Gamma}\dot{\boldsymbol{D}} + p\boldsymbol{L} - \dot{p}\mathbf{I} \tag{18}$$

$$\dot{\boldsymbol{E}} = \boldsymbol{\Gamma}^{\mathrm{T}}\boldsymbol{L} + \boldsymbol{K}\dot{\boldsymbol{D}} \tag{19}$$

where $\boldsymbol{L} = \operatorname{grad} \boldsymbol{u}$ is the displacement gradient, $\boldsymbol{A}$, $\boldsymbol{\Gamma}$, and $\boldsymbol{K}$ are the fourth-, third- and second-order electro-elastic moduli tensors, respectively, which can be defined in terms of the energy function Σ of an incompressible material as follows:

$$\boldsymbol{A} = \boldsymbol{F}\boldsymbol{F}\frac{\partial^2\Sigma}{\partial\boldsymbol{F}\partial\boldsymbol{F}}, \boldsymbol{\Gamma} = \boldsymbol{F}\boldsymbol{F}^{-1}\frac{\partial^2\Sigma}{\partial\boldsymbol{F}\partial\boldsymbol{D}_L}, \boldsymbol{\Gamma}^T = \boldsymbol{F}^{-1}\boldsymbol{F}\frac{\partial^2\Sigma}{\partial\boldsymbol{D}_L\partial\boldsymbol{F}},$$
$$\mathrm{K} = \boldsymbol{F}^{-1}\boldsymbol{F}^{-1}\frac{\partial^2\Sigma}{\partial\boldsymbol{D}_L\partial\boldsymbol{D}_L} \tag{20}$$

For the symmetrical case, $\boldsymbol{\Gamma} = \boldsymbol{\Gamma}^{\mathrm{T}}$. The previous expression reads in the component form:

$$A_{piqj} = F_{p\alpha}F_{q\beta}\frac{\partial^2\Sigma}{\partial F_{i\alpha}\partial F_{j\beta}}, \Gamma_{pi|q} = F_{p\alpha}F_{\beta q}^{-1}\frac{\partial^2\Sigma}{\partial F_{i\alpha}\partial D_{L\beta}},$$
$$K_{ij} = F_{\alpha i}^{-1}F_{\beta j}^{-1}\frac{\partial^2\Sigma}{\partial D_{L\alpha}\partial D_{L\beta}} \tag{21}$$

3.2 Incremental Governing Equations and Boundary Conditions. The components of the displacement gradient L_{ij} and incremental incompressibility condition are defined in the case of axisymmetric incremental motion and incremental displacement $\boldsymbol{u} = \boldsymbol{u}(r, z, t) = u_r(r, z, t)\boldsymbol{e}_r + u_z(r, z, t)\boldsymbol{e}_z$ as follows:

$$\boldsymbol{L} = \begin{bmatrix} L_{rr} & 0 & L_{rz} \\ 0 & L_{\theta\theta} & 0 \\ L_{zr} & 0 & L_{zz} \end{bmatrix} = \begin{bmatrix} \dfrac{\partial u_r}{\partial r} & 0 & \dfrac{\partial u_r}{\partial z} \\ 0 & \dfrac{u_r}{r} & 0 \\ \dfrac{\partial u_z}{\partial r} & 0 & \dfrac{\partial u_z}{\partial z} \end{bmatrix}, \tag{22}$$

where $\boldsymbol{e}_r$ and $\boldsymbol{e}_z$ are the basis vectors in the radial and axial directions, respectively. Due to the incompressibility of the material, we have

$$\operatorname{div} \boldsymbol{u} = \operatorname{tr} \boldsymbol{L} = L_{rr} + L_{\theta\theta} + L_{zz} = \frac{\partial u_r}{\partial r} + \frac{u_r}{r} + \frac{\partial u_z}{\partial z} = 0 \tag{23}$$

The incremental Maxwell's equations and equations of motion of the soft DEA tube are given as follows:

$$\operatorname{div} \dot{\boldsymbol{D}} = 0, \quad \operatorname{curl} \dot{\boldsymbol{E}} = 0, \quad \operatorname{div} \dot{\boldsymbol{T}} = \rho \boldsymbol{u}_{,tt} \tag{24}$$

which have the component forms as follows:

$$\begin{aligned} &\dot{D}_{r,r} + \dot{D}_{z,z} = 0, \\ &\dot{E}_{r,z} - \dot{E}_{z,r} = 0, \\ &\dot{T}_{rr,r} + \frac{1}{r}(\dot{T}_{rr} - \dot{T}_{\theta\theta}) + \dot{T}_{rz,z} = \rho u_{r,tt}, \\ &\dot{T}_{zr,r} + \frac{1}{r}\dot{T}_{zr} + \dot{T}_{zz,z} = \rho u_{z,tt} \end{aligned} \tag{25}$$

Moreover, the incremental electric field derived from Eq. (25)$_2$ reads

$$\dot{E} = -\operatorname{grad} \dot{\varphi} \tag{26}$$

where $\dot{\varphi}$ is the incremental electric potential.

The corresponding incremental mechanical and electric boundary conditions for invariant applied voltage and pressure at both ends $z = \pm l/2$, and the faces $r = r_i$ and $r = r_o$ take the following expressions:

$$u_z = \dot{T}_{rz} = 0 \quad (z = \pm l/2) \tag{27}$$

$$\dot{T}_{rr} = P_f L_{rr}, \quad \dot{T}_{rz} = P_f L_{rz}, \quad \dot{\varphi} = 0 \quad (r = r_i) \tag{28}$$

$$\dot{T}_{rr} = P_o L_{rr}, \quad \dot{T}_{rz} = P_o L_{rz}, \quad \dot{\varphi} = 0 \quad (r = r_o) \tag{29}$$

4 Numerical Calculations

4.1 Material Model. By considering the Gent dielectric model [42], the energy function required for solutions to elastic problems involving large nonuniform deformations defines

$$\Sigma = -\frac{1}{2}\mu G \log\left[1 - (I_1 - 3)/G\right] + \frac{1}{2}\varepsilon^{-1}I_5 \tag{30}$$

where μ is the initial shear modulus and G is the Gent constant. Thus, we determine the electro-elastic moduli according to the energy functions mentioned in Eq. (9):

$$\begin{aligned} &A_{piqj} = 4W_{11}b_{ip}b_{jq} + 2W_1\delta_{ij}b_{pq} + \varepsilon^{-1}\delta_{ij}D_pD_q, \\ &\Gamma_{pi|q} = \varepsilon^{-1}(\delta_{pq}D_i + \delta_{iq}D_p), \quad K_{ij} = \varepsilon^{-1}\delta_{ij} \end{aligned} \tag{31}$$

where $W_1 = \partial W/\partial I_1$, $W_{11} = \partial^2 W/\partial I_1^2$.

We use the following characters for defining different moduli [25]:

$$\begin{aligned} &a = A_{zrzr}, 2b = A_{rrrr} + A_{zzzz} - 2A_{rrzz} - 2A_{rzzr}, c = A_{rzrz}, d = \Gamma_{zr|z}, \\ &g = 2A_{rrzz} - 2A_{\theta\theta zz} + A_{\theta\theta\theta\theta} - A_{rrrr}, q = A_{rrrr} - A_{rrzz} + A_{\theta\theta zz} - A_{rr\theta\theta} - A_{rzzr} \end{aligned} \tag{32}$$

Then, for the Gent model in Eq. (30), we obtain

$$\begin{aligned} &A_{rzzr} = 0, \Gamma_{zz|r} = \Gamma_{\theta\theta|r} = 0, K_{rr} = K_{zz} = \varepsilon^{-1}, \Gamma_{rr|r} = 2d, \\ &a = 2W_1\lambda_z^2, 2b = 4W_{11}(\lambda_z^2 - \lambda_r^2)^2 + 2W_1(\lambda_z^2 + \lambda_r^2) + dD_r, \\ &d = \varepsilon^{-1}D_r, g = 4W_{11}\lambda_r^4[(1 - \lambda^4\lambda_z^2)(2\lambda^2\lambda_z^4 - \lambda^4\lambda_z^2 - 1)] - 2W_1\lambda_r^2(1 - \lambda^4\lambda_z^2) - dD_r, \\ &q = 4W_{11}\lambda_r^4[(1 - \lambda^2\lambda_z^4)(1 - \lambda^4\lambda_z^2)] + 2W_1\lambda_r^2 + dD_r, c = 2W_1\lambda_r^2 + dD_r \end{aligned} \tag{33}$$

4.2 State-Space Method. SSM is an effective approach for eigenvalue problems to solve physical systems represented by linearized differential equations through a set of state vectors [43]. The state vectors can be defined by presumed functions to be employed in the linearized incremental solutions as follows:

$$\begin{aligned} &u_r = R_i\bar{u}_r(\hat{r})\cos(\alpha z)\cdot e^{i\omega t}, u_z = R_i\bar{u}_z(\hat{r})\sin(\alpha z)\cdot e^{i\omega t}, \dot{\varphi} = R_i\sqrt{\mu/\varepsilon}\Phi(\hat{r})\cos(\alpha z)\cdot e^{i\omega t}, \\ &\dot{T}_{rr} = \mu\bar{T}_{rr}(\hat{r})\cos(\alpha z)\cdot e^{i\omega t}, \dot{T}_{rz} = \mu\bar{T}_{rz}(\hat{r})\sin(\alpha z)\cdot e^{i\omega t}, \dot{D}_r = \sqrt{\mu\cdot\varepsilon}\bar{D}_r(\hat{r})\cos(\alpha z)\cdot e^{i\omega t} \end{aligned} \tag{34}$$

$\bar{u}_r$, $\bar{u}_z$, Φ, $\bar{T}_{rr}$, $\bar{T}_{rz}$, and $\bar{D}_r$ are scalar functions of $\hat{r} = r/R_i$ only. $i = \sqrt{-1}$ is the imaginary unit. By rearranging the incremental governing equations in the following form

$$\frac{\partial\boldsymbol{\mathcal{Y}}(r)}{\partial r} = \boldsymbol{\mathcal{M}}(r)\cdot\boldsymbol{\mathcal{Y}}(r) \tag{35}$$

we have $\mathcal{Y}(r)$ and $\mathcal{M}(r)$, the state vector and matrix, respectively, given

$$\mathcal{Y}(r)=\begin{bmatrix} u_r \\ u_z \\ \dot{\varphi} \\ \dot{T}_{rr} \\ \dot{T}_{rz} \\ \dot{D}_r \end{bmatrix}, \mathcal{M}(r)=\begin{bmatrix} -\frac{1}{r} & -\frac{\partial}{\partial z} & 0 & 0 & 0 & 0 \\ -\delta_1\frac{\partial}{\partial z} & 0 & \delta_2\frac{\partial}{\partial z} & 0 & \delta_3 & 0 \\ \frac{\delta_4}{r} & \delta_4\frac{\partial}{\partial z} & 0 & 0 & 0 & -\varepsilon^{-1} \\ \frac{\beta_1}{r^2}-\beta_2\frac{\partial^2}{\partial z^2}+\rho\frac{\partial^2}{\partial t^2} & \frac{\beta_3}{r}\frac{\partial}{\partial z} & -\delta_2\beta_4\frac{\partial^2}{\partial z^2} & 0 & -\delta_1\frac{\partial}{\partial z} & -\frac{\delta_4}{r} \\ -\frac{\beta_3}{r}\frac{\partial}{\partial z} & \frac{\partial^2}{\partial t^2}-\beta_5\frac{\partial^2}{\partial z^2} & 0 & -\frac{\partial}{\partial z} & -\frac{1}{r} & \delta_4\frac{\partial}{\partial z} \\ -\delta_2\beta_4\frac{\partial^2}{\partial z^2} & 0 & \delta_5\frac{\partial^2}{\partial z^2} & 0 & \delta_2\frac{\partial}{\partial z} & -\frac{1}{r} \end{bmatrix} \tag{36}$$

where ρ is the density of the soft DEA tube in the deformed configuration, and

$$\begin{aligned} &\delta_1=\frac{p-\varepsilon d^2}{c-\varepsilon d^2}, \delta_2=\frac{\varepsilon d}{c-\varepsilon d^2}, \delta_3=\frac{1}{c-\varepsilon d^2}, \delta_4=2d, \\ &\delta_5=\frac{\varepsilon c}{c-\varepsilon d^2}, \beta_1=g+2q+2p, \\ &\beta_2=a-\varepsilon d^2-\frac{(p-\varepsilon d^2)^2}{c-\varepsilon d^2}, \beta_3=q+p, \\ &\beta_4=p-c, \beta_5=2b+2p \end{aligned} \tag{37}$$

To ease the solutions processes [44], we adopt the dimensional analysis, such that the dimensionless quantities employed for the incremental quantities read

$$\begin{aligned} &\hat{A}=\frac{A}{\mu}, \hat{\Gamma}=\sqrt{\frac{\varepsilon}{\mu}}\Gamma, \hat{K}=\varepsilon K, \hat{V}=\sqrt{\frac{\varepsilon}{\mu}}\frac{V}{R_i}, \hat{a}=\frac{a}{\mu}, \\ &\hat{b}=\frac{b}{\mu}, \hat{c}=\frac{c}{\mu}, \hat{d}=\sqrt{\frac{\varepsilon}{\mu}}d, \hat{p}=\frac{p}{\mu}, \hat{g}=\frac{g}{\mu}, \hat{q}=\frac{q}{\mu}, \\ &\hat{r}=\frac{r}{R_i}, \Delta\hat{P}=\frac{\Delta P}{\mu}, \hat{\alpha}=\alpha R_i, \zeta=z/l, B(\hat{r})=\frac{B(r)}{R_i}, \\ &\Omega=\omega R_i/\sqrt{\mu/\rho_s}, \hat{P}_f=\frac{P_f}{\mu}=\frac{-\Omega^2}{R_i}B(\hat{r})(\rho_f/\rho_s), \hat{\chi}=\chi R_i=\Omega\left(\frac{c_s}{c_f}\right)-\hat{\alpha} \end{aligned} \tag{38}$$

where ρ_s is the DEA density in the undeformed configuration and $c_s=\sqrt{\mu/\rho_s}$ is the elastic wave velocity in the soft DEA tube. For a homogeneous material, $\rho=\rho_s$. Thus, the dimensionless incremental governing equations

$$\frac{\partial\bar{\mathcal{Y}}(\hat{r})}{\partial\hat{r}}=\bar{\mathcal{M}}(\hat{r})\cdot\bar{\mathcal{Y}}(\hat{r}) \tag{39}$$

where $\bar{\mathcal{Y}}(\hat{r})=\begin{bmatrix}\bar{u}_r & \bar{u}_z & \Phi & \bar{T}_{rr} & \bar{T}_{rz} & \bar{D}_r\end{bmatrix}^{\mathrm{T}}$ is the dimensionless state vector. The dimensionless state matrix $\bar{\mathcal{M}}(\hat{r})$

$$\bar{\mathcal{M}}(\hat{r})=\begin{bmatrix} -\frac{1}{\hat{r}} & -\hat{\alpha} & 0 & 0 & 0 & 0 \\ \hat{\alpha}\bar{\delta}_1 & 0 & -\hat{\alpha}\bar{\delta}_2 & 0 & \bar{\delta}_3 & 0 \\ \frac{\bar{\delta}_4}{\hat{r}} & \hat{\alpha}\bar{\delta}_4 & 0 & 0 & 0 & -1 \\ \frac{\bar{\beta}_1}{\hat{r}}+\hat{\alpha}^2\bar{\beta}_2-\frac{\rho}{\rho_s}\Omega^2 & \hat{\alpha}\frac{\bar{\beta}_3}{\hat{r}} & \hat{\alpha}^2\bar{\delta}_2\bar{\beta}_4 & 0 & -\hat{\alpha}\bar{\delta}_1 & -\frac{\bar{\delta}_4}{\hat{r}} \\ \hat{\alpha}^2\frac{\bar{\beta}_3}{\hat{r}} & \hat{\alpha}^2\bar{\beta}_5-\frac{\rho}{\rho_s}\Omega^2 & 0 & \hat{\alpha} & -\frac{1}{r} & -\hat{\alpha}\bar{\delta}_4 \\ \hat{\alpha}^2\bar{\delta}_2\bar{\beta}_4 & 0 & -\hat{\alpha}^2\bar{\delta}_5 & 0 & \hat{\alpha}\bar{\delta}_2 & -\frac{1}{\hat{r}} \end{bmatrix} \tag{40}$$

with

$$\bar{\delta}_1 = \delta_1, \bar{\delta}_2 = \delta_2\sqrt{\frac{\mu}{\varepsilon}}, \bar{\delta}_3 = \mu\delta_3, \bar{\delta}_4 = \delta_4\sqrt{\frac{\varepsilon}{\mu}},$$
$$\bar{\delta}_5 = \frac{\delta_5}{\varepsilon}, \bar{\beta}_j = \frac{\beta_j}{\mu}\ (j = 1, 2, \ldots, 5) \tag{41}$$

Combined with the SSM, we use the approximate laminate technique for having constant coefficients and enhanced results with a relative error $\epsilon \lesssim 10^{-3}$ [45]. That can be accomplished by dividing the tube thickness in the cylindrical coordinates into 30 sublayers so that the inner and outer radii of each sublayer can be calculated as follows:

$$r_{k-1} = r_i + (k-1)\frac{h}{N} \le r \le r_k = r_i + k\frac{h}{N} \tag{42}$$

where N is the total number of DEA sublayers, and k is the order of the sublayer ($k = 1, 2, \ldots, N$).

By taking the average of radii of the sublayer after normalizing the basic variables to R_i, we obtain

$$\hat{r}_m = \frac{r_i}{R_i} + (2k-1)\frac{h}{2NR_i} \tag{43}$$

where $m = (2k-1)/2$, is the order of the mid-sublayer. Accordingly, the solutions of the of the differential equations system Eq. (39) read

$$\bar{\boldsymbol{\mathcal{Y}}}(\hat{r}_o) = \bar{\mathbf{A}}\bar{\boldsymbol{\mathcal{Y}}}(\hat{r}_i),\ \bar{\mathbf{A}} = \Pi_{k=N_i}^{1}\mathrm{Exp}[(\hat{r}_k - \hat{r}_{k-1})\cdot\bar{\boldsymbol{\mathcal{M}}}(\hat{r}_m)] \tag{44}$$

where $\bar{\boldsymbol{\mathcal{Y}}}(\hat{r}_i)$, $\bar{\boldsymbol{\mathcal{Y}}}(\hat{r}_o)$ are the dimensionless state vectors at the inner and outer surfaces of the soft DEA tube, respectively. $\bar{\mathbf{A}}$ is the dimensionless transfer matrix of coefficients. $\bar{\boldsymbol{\mathcal{M}}}(\hat{r}_m)$ is the dimensionless state matrix of coefficients at the considered mid-sublayer in the soft DEA tube.

From the determinant of coefficients and after applying the incremental boundary conditions in Eqs. (28) and (29), we obtain the characteristic equation:

$$\begin{vmatrix} \left(\bar{A}_{31} - \frac{\Delta\hat{P}}{\hat{r}}\bar{A}_{34} - \hat{\alpha}\cdot\Delta\hat{P}\cdot\bar{A}_{35}\right) & (\bar{A}_{32} - \hat{\alpha}\cdot\Delta\hat{P}\cdot\bar{A}_{34}) & \bar{A}_{36} \\ \left(\bar{A}_{41} - \frac{\Delta\hat{P}}{\hat{r}}\bar{A}_{44} - \hat{\alpha}\cdot\Delta\hat{P}\cdot\bar{A}_{45}\right) & (\bar{A}_{42} - \hat{\alpha}\cdot\Delta\hat{P}\cdot\bar{A}_{44}) & \bar{A}_{46} \\ \left(\bar{A}_{51} - \frac{\Delta\hat{P}}{\hat{r}}\bar{A}_{54} - \hat{\alpha}\cdot\Delta\hat{P}\cdot\bar{A}_{55}\right) & (\bar{A}_{52} - \hat{\alpha}\cdot\Delta\hat{P}\cdot\bar{A}_{54}) & \bar{A}_{56} \end{vmatrix} = 0 \tag{45}$$

where $\bar{A}_{ij}$ are the elements of the dimensionless transfer matrix of coefficients $\bar{\mathbf{A}}$.

5 Results and Discussion

A homogeneous soft DEA tube under radial voltage and external pressure is examined in this section by considering the aspect ratio of the tube $\eta = 0.85$ and a finite-length $L = 10R_o$. The axial stretch is fixed $\lambda_z = 1.2$, and then, the associated critical circumferential stretch for incompressible materials is $\lambda_{i_{cr}} = \lambda_z^{-1/2} \approx 0.913$, unless otherwise stated. The tube undergoes external pressure at its outer face, while its inner face is traction free. Also, the voltage is applied between the mounted electrodes on the inner and outer faces. The wavenumber's first three modes ($n = 1, 2, 3$) are also considered. We use the Gent model with $G = 97.2$ to discuss material behavior.

5.1 Vibration Characteristics of the Fluid-Free Soft Dielectric Elastomer Actuator Tube.

Figure 2 displays the critical voltage corresponding to the cutoff frequency or phase velocity beyond which the real values vanish for the subcritical and overcritical circumferential stretches $\lambda_i = 0.9$, 1.1, respectively.

For both values of the circumferential stretch, the higher modes have higher frequencies and lower phase velocities, approaching zero when we apply the critical voltage. Moving into higher mode numbers decreases the admissible value of the applied voltage. The critical value of the applied voltage for the overcritical circumferential stretch is less than that for the subcritical case. That is, the overcritical circumferential stretch attenuates the capability of the soft DEA tube to receive more voltage and takes it toward a failure developed by an axisymmetric instability.

To have a clear idea about the vibrational behavior in the fluid-free soft DEA tube, we can observe from Fig. 3 that the frequency and phase velocity for higher applied voltages tend to zero with higher mode numbers, especially if the circumferential stretch is overcritical. In the latter case, the values vanish even in the range of lower mode numbers. On the other hand, for the purely elastic cases and higher mode numbers ($n > 5$), the frequency of the overcritical case takes higher values than those of the subcritical case. The same behavior can be observed for the phase velocity. The transition region, where the phase velocity moves from higher to lower velocities, is broad and smooth in the purely elastic case and ends with a constant and stable value. In contrast, for increasing mode numbers at higher applied voltages and the subcritical and overcritical cases, the transition region of the phase velocity becomes narrow with a rapid decrease in values.

If we consider the critical case of the axial stretch $\lambda_z = 1.2$ and $\lambda_{i_{cr}} \approx 0.913$, accordingly, we can capture the role of the applied voltage in controlling the vibrational behavior in the fluid-free soft DEA tube, as in Fig. 4. Increasing the applied voltage causes a reduction of the resulting frequency and phase velocity. It accelerates the occurrence of axisymmetric instability, particularly with higher modes. In addition, the transition region in the phase velocity becomes smaller with higher applied voltages and is accompanied

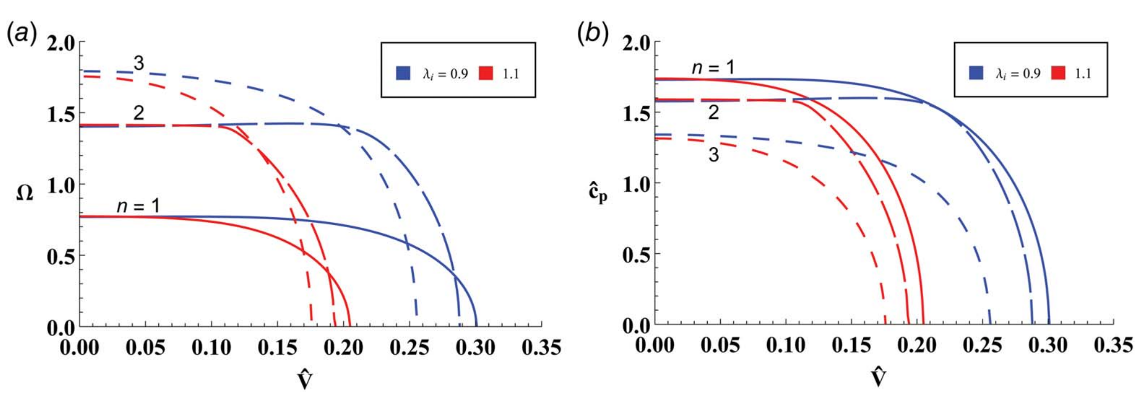

Fig. 2 The first three modes of the (a) normalized frequency Ω and (b) phase velocity $\hat{c}_p = \Omega/\hat{\alpha}$ of the fluid-free soft DEA tube for $\lambda_i = 0.9$, 1.1, and $\lambda_z = 1.2$, under different values of the applied voltage

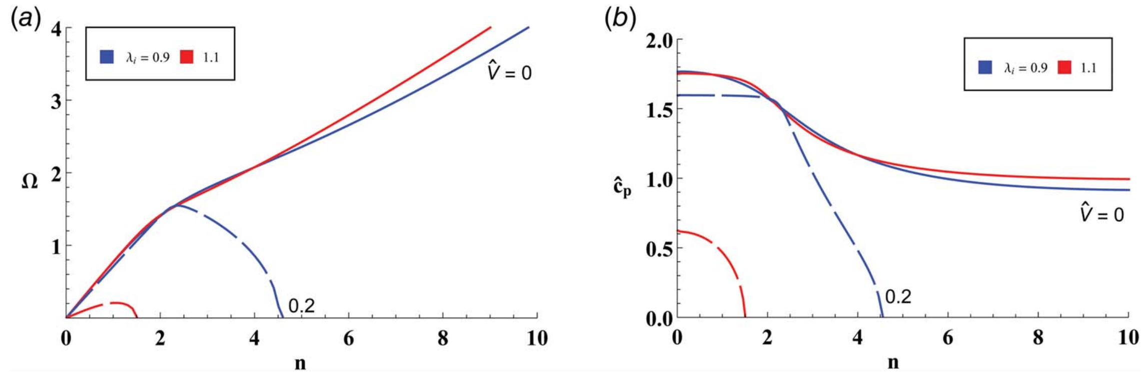

Fig. 3 (*a*) Dimensionless frequency Ω and (*b*) phase velocity $\hat{c}_p = \Omega/\hat{\alpha}$ of the fluid-free soft DEA tube versus the dimensionless axial mode number for $\lambda_z = 1.2$, and $\lambda_i = 0.9$, 1.1, with values of the applied voltage $\hat{V} = 0$, 0.2

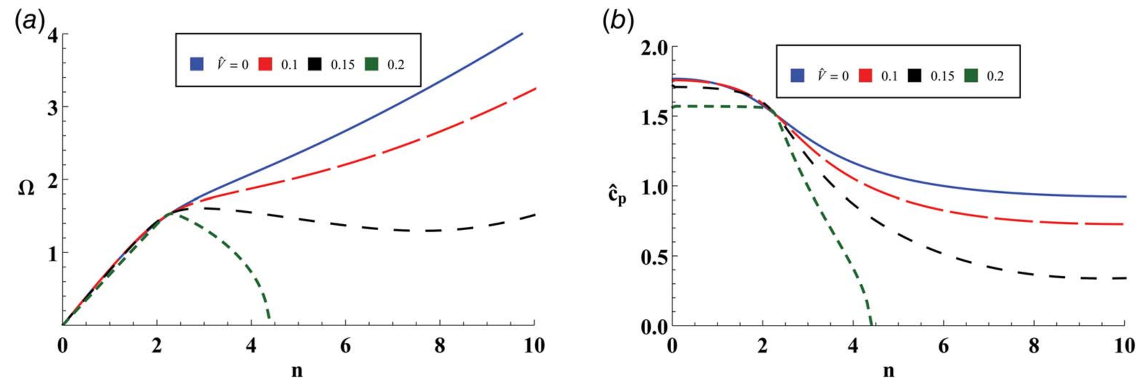

Fig. 4 (*a*) Dimensionless frequency Ω and (*b*) phase velocity $\hat{c}_p = \Omega/\hat{\alpha}$ of the fluid-free soft DEA tube versus the dimensionless axial mode number for $\lambda_z = 1.2$, and critical $\lambda_{i_{cr}} \approx 0.913$, with different values of the applied voltage $\hat{V} = 0,\ 0.1,\ 0.15,\ \ 0.2$

by a quick drop in values and the development of axisymmetric instability.

5.2 Vibration Characteristics of the Fluid-Filled Soft Dielectric Elastomer Actuator Tube. With the same assumptions mentioned earlier in this section, i.e., $\eta = 0.85$, $L = 10R_o$, and $\lambda_z = 1.2$, the soft DEA tube is subject to external pressure at its outer face, and the inner face is in contact with an inviscid compressible fluid. Both faces are mounted to flexible electrodes to generate the voltage applied to the tube. In addition, it is assumed that the fluid-to-DEA density ratio remains fixed at $\hat{\rho}_{fs} = \rho_f/\rho_s = 0.13$, while the ratio of elastic wave velocity in the fluid-to-DEA remains constant at $\hat{c}_{fs} = c_f/c_s = 0.27$. The effect of purely applied voltage on the frequency and phase velocity of the fluid-filled soft DEA tube are explicitly illustrated in Fig. 5.

Similar to the fluid-free case, the higher frequencies are obtained as we go up in the modes. In turn, lower phase velocities appear with these higher modes. The critical value of the applied voltage, where the soft DEA tube reaches the axisymmetric instability at zero frequency or zero phase velocity, arises earlier in the overcritical case due to the combination effect of applied voltage and stretch. It also gives rise to an overthinning of the soft DEA tube. However, the frequency and phase velocity reappear with increasing the applied voltage, specifically in the higher modes of overcritical stretch (here, $n = 3$). Those recorded values can be attributed to the presence of the fluid. The pressure induced by the fluid and exerted on the inner surface of the DEA prevents any surface instability, which may develop on that surface when there is no fluid. In this sense, we may also consider that the fluid can endow the system with a partial self-healing capability. Nevertheless, when the fluid is not placed between the electrodes, the system cannot resist the instability resulting from the overthinning of the soft DEA, which is also caused by applying a sufficiently high voltage.

The notable decrease in the frequency and phase velocity in Fig. 6 can be compared easily to the obtained values in Fig. 3 for the fluid-free soft DEA tube. That is owing to the added mass effect induced by the inviscid compressible fluid, which emerges as an additional reduction in the frequency and phase velocity in cases both with and without applied voltage. The reduction becomes more as we move to higher modes, particularly with overcritical stretch, as shown in Fig. 6. The transition region in phase velocity sharply decreases compared to the fluid-free case. Also, the higher applied voltages contribute to the early occurrence of axisymmetric instability with higher modes. It could extend to the lower modes in the case of the overcritical circumferential stretch, with which the frequency and phase velocity values decrease more. The observed effect of the added mass against the axisymmetric instability's development is shown in Fig. 7. Although the added mass reduces the frequency and phase velocity, it also hinders the early onset of axisymmetric instability when increasing the applied voltage. We figured out that by comparing the obtained results for $\hat{V} = 0.15$ in Fig. 7 with those in Fig. 4. Nevertheless, the role of added mass against early axisymmetric instability dwindles in front of the ongoing rise in the applied voltage due to electric dominance over the added mass.

5.3 Parametric Study of the Inviscid Compressible Fluid-Filled Soft Dielectric Elastomer Actuator Tube. In this section, we investigate the variation effect of the parameters involved in the fluid-filled soft DEA tube. In fact, the parametric

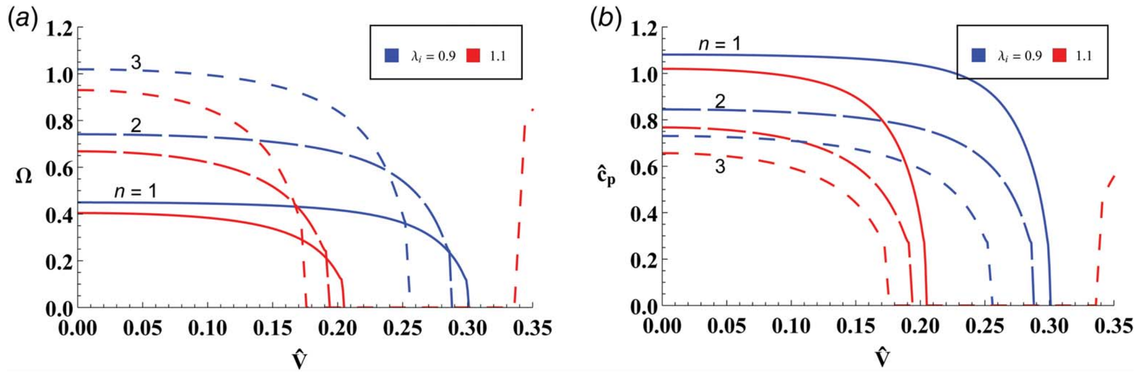

Fig. 5 The first three modes of the (*a*) normalized frequency Ω and (*b*) phase velocity $\hat{c}_p = \Omega/\hat{\alpha}$ of the fluid-filled soft DEA tube for $\lambda_i = 0.9,\ 1.1$, and $\lambda_z = 1.2$, under different values of the applied voltage

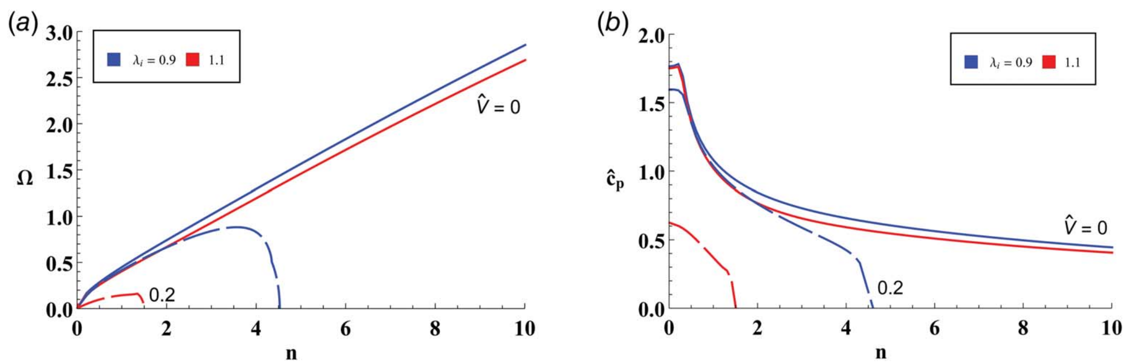

Fig. 6 (*a*) Dimensionless frequency Ω and (*b*) phase velocity $\hat{c}_p = \Omega/\hat{\alpha}$ of the fluid-filled soft DEA tube versus the axial mode number for $\lambda_z = 1.2$, and $\lambda_i = 0.9,\ 1.1$, with values of the applied voltage $\hat{V} = 0,\ 0.2$

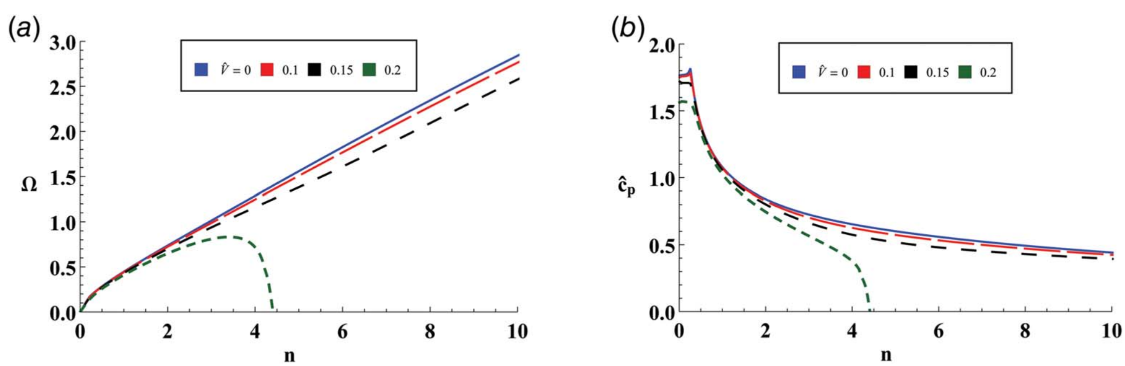

Fig. 7 (*a*) Dimensionless frequency Ω and (*b*) phase velocity $\hat{c}_p = \Omega/\hat{\alpha}$ of the fluid-filled soft DEA tube versus the dimensionless axial mode number for $\lambda_z = 1.2$, and critical $\lambda_{i_{cr}} \approx 0.913$, with different values of the applied voltage $\hat{V} = 0,\ 0.1,\ 0.15,\ 0.2$

study provides a helpful guideline for optimizing and seeking the best performance of the operated soft DEA based on the application needs, such as the fluid properties (velocity and density), voltage range, thickness of the soft DEA, and frequency of operation.

The ratio of elastic wave velocity in the fluid to that one in the soft DEA tube $\hat{c}_{fs}$, the ratio of fluid density to the soft DEA tube density $\hat{\rho}_{fs}$, and the thickness ratio of the soft DEA tube to its inner radius h/R_i are the keystones of our investigation for a fixed axial stretch $\lambda_z = 1.2$, along with the associated subcritical and overcritical circumferential stretches $\lambda_i = 0.9,\ 1.1$, respectively. Furthermore, we consider the purely elastic case, where $\hat{V} = 0$, and the applied voltage case for $\hat{V} = 0.15$ for subcritical and overcritical circumferential stretches.

The first three modes of frequency versus $\hat{c}_{fs}$ are demonstrated in Fig. 8. With increasing $\hat{c}_{fs}$, higher mode frequencies will increase both for a purely elastic case and applied voltage. Although the frequency also grows with increasing $\hat{c}_{fs}$ for the lowest mode, when the elastic wave velocity in the fluid approaches the one in the soft DEA tube, the frequency converges to a fixed, stable value. Applying voltage, particularly accompanied by an overcritical circumferential stretch, reduces the frequency compared to the frequency resulting from the subcritical circumferential stretch and purely elastic cases.

By examining the effect of $\hat{\rho}_{fs}$ on the resulting frequency, we obtain Fig. 9. In the higher modes, a notable decrease in frequency appears when moving to higher values of $\hat{\rho}_{fs}$. This decline is relatively small in the lowest mode and nearly approaches a constant

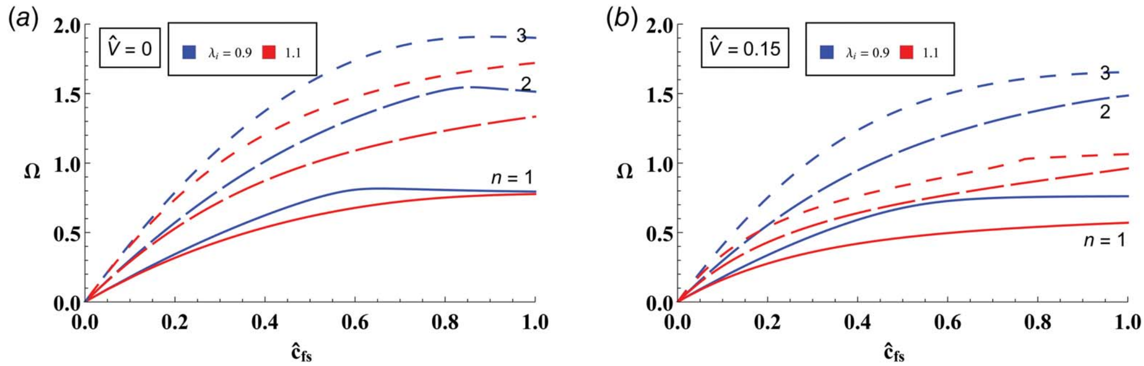

Fig. 8 Normalized frequency of the fluid-filled soft DEA tube versus $\hat{c}_{fs}$ for (*a*) $\hat{V} = 0$ and (*b*) $\hat{V} = 0.15$; with $\lambda_z = 1.2$, $\lambda_i = 0.9$, 1.1, and $\hat{\rho}_{fs} = 0.13$

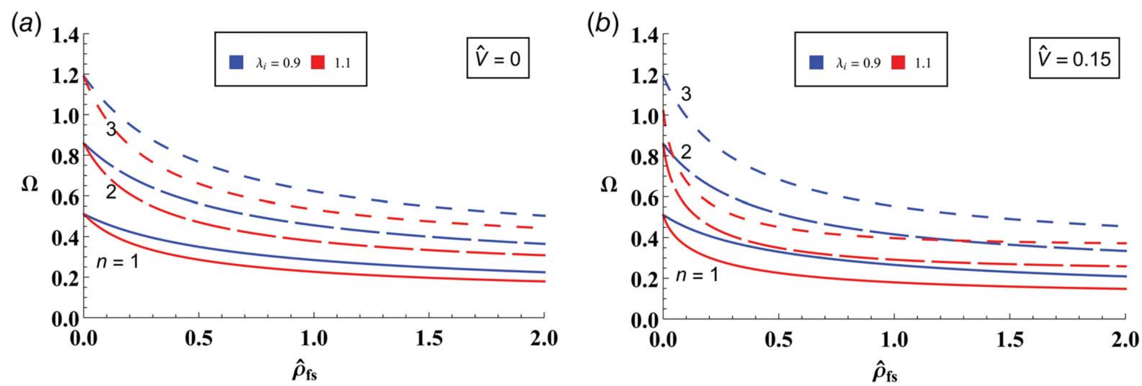

Fig. 9 Normalized frequency of the fluid-filled soft DEA tube versus $\hat{\rho}_{fs}$ for (*a*) $\hat{V} = 0$ and (*b*) $\hat{V} = 0.15$, with $\lambda_z = 1.2$, $\lambda_i = 0.9$, 1.1, and $\hat{c}_{fs} = 0.27$

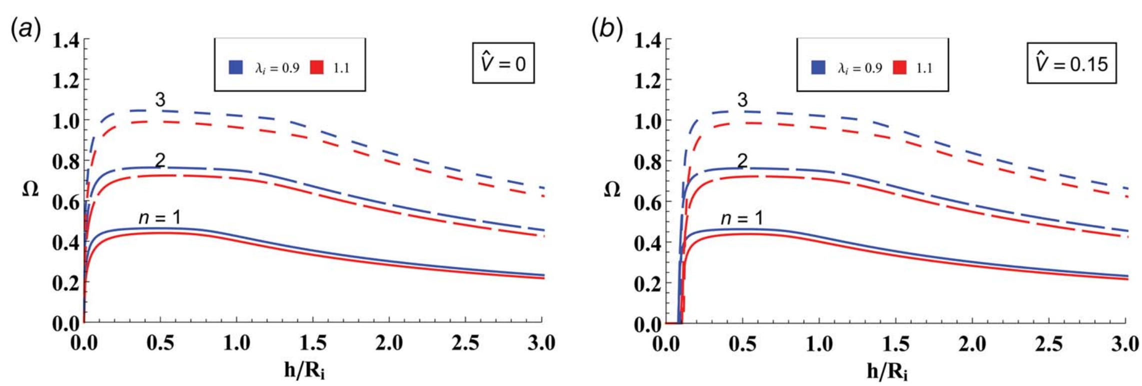

Fig. 10 Normalized frequency of the fluid-filled soft DEA tube versus h/R_i for (*a*) $\hat{V} = 0$ and (*b*) $\hat{V} = 0.15$, with $\lambda_z = 1.2$, $\lambda_i = 0.9$, 1.1, $\hat{\rho}_{fs} = 0.13$, and $\hat{c}_{fs} = 0.27$

value when the fluid density exceeds the soft DEA tube's density. The overcritical circumferential stretch also minimizes frequency values, specifically with higher modes and applied voltage, where the fluid density is much lower than that of the soft DEA tube, as shown in Fig. 9(*b*). Apart from the latter case, the applied voltage does not remarkably affect the frequency with a varying $\hat{\rho}_{fs}$, especially for subcritical circumferential stretch.

To understand the role of the thickness of the soft DEA tube in the obtained frequencies, we observe that Fig. 10 shows a high frequency for a very thin-walled tube. As thickness increases, the frequency stabilizes until the thickness approximately equals the tube's inner radius or slightly more for higher modes. Beyond this limit, a smooth drop in the frequency occurs such that its values return to smaller values for a very thick tube. This behavior holds regardless of whether the case is purely elastic or involves applied voltage, subcritical, or overcritical circumferential stretch. However, higher applied voltages require increased thickness in soft DEA tubes, as evidenced by a dislodging toward larger values compared to the purely elastic case. The difference in values between the cases of subcritical and overcritical circumferential stretch is slight and can be negligible for the lowest mode of frequencies.

6 Conclusions

This work used the Gent model to describe the material behavior and investigate the axisymmetric vibration of an inviscid compressible fluid-filled soft DEA tube. The soft DEA tube was a thin-walled structure that underwent an electric voltage generated by mounted electrodes on its inner and outer faces, along with subcritical or overcritical circumferential pre-stretches. External pressure was applied at the outer surface of the tube, while at the inner surface, the tube was in contact with an inviscid compressible fluid. We considered the impact of various parameters on the resulting frequencies, such as the ratio of elastic wave velocity in the fluid to its counterpart in the soft DEA tube, the ratio of fluid density to soft DEA tube density, and the effect of tube thickness.

The results of the characteristic equation showed higher frequencies with the higher modes when applying higher voltages. In contrast, lower phase velocities were caught with the higher modes for the same case. The early axisymmetric instability of the soft DEA tube was attributed to the combination of the higher applied voltage and overcritical circumferential stretch, which could be detected through the cutoff frequencies. Nevertheless, the fluid allowed the soft DEA tube to partially self-heal, whereas the instability induced by the overthinning of the soft DEA was still irresistible. The filled inviscid compressible fluid reduced the frequency and phase velocity over the range of axial modes compared to the fluid-free case. It was traced back to the added mass effect. The added mass confronted the early occurrence of axisymmetric instability with the increasing applied voltage. However, the higher applied voltage remained dominant over the added mass effect.

The frequency increased with the rising ratio of elastic wave velocity in the fluid to its counterpart in the soft DEA tube, while it gave stability in value when the elastic wave velocity in the fluid approached its peer in the soft DEA tube for the lowest mode. Meanwhile, the frequency kept rising with higher modes. Increasing the fluid density decreased the resulting frequency over all modes. When the fluid density was greater than or equal to the soft DEA tube density, the frequency converged almost to a fixed value. In the higher modes, the overcritical stretch at an applied voltage and the DEA tube's huge density reduced the frequency compared to the purely elastic case. That was the only case where the applied voltage affected the frequency with varying densities. When the thickness of the soft DEA tube raised over its inner radius, the frequency had a smooth decrease in values. The frequency results of the subcritical and overcritical cases differed marginally, with a dislodging in the initial required thickness when applying the voltage. This dislodging could increase when higher voltages were applied, suggesting the demand for a thicker tube to withstand the higher applied voltage.

The achieved work gives a comprehensive idea about the vibrational behavior of the soft DEA tube in contact with fluid, which has promising applications, such as robotics, prosthetics, and gripping systems, where fast operation, large deformation, high performance, and durability are required.

Funding Data

- National Natural Science Foundation of China (Grant Nos. 11872329, 12192210, and 12192211).
- The 111 Project (Grant No. B21034).
- Natural Science Foundation of Zhejiang Province (Grant No. LD21A020001).
- Partial support from the Shenzhen Scientific and Technological Fund for R&D, China (Grant No. 2021Szvup152).

Conflict of Interest

There are no conflicts of interest.

Data Availability Statement

The authors attest that all data for this study are included in the paper.

References

[1] Bathe, M., and Kamm, R. D., 1999, "A Fluid–Structure Interaction Finite Element Analysis of Pulsatile Blood Flow Through a Compliant Stenotic Artery," ASME J. Biomech. Eng., **121**(4), pp. 361–369.
[2] Carpi, F., 2016, *Electromechanically Active Polymers*, Springer, Cham, Switzerland.
[3] Shankar, R., Ghosh, T. K., and Spontak, R. J., 2007, "Dielectric Elastomers as Next-Generation Polymeric Actuators," Soft Matter, **3**(9), pp. 1116–1129.
[4] Brochu, P., and Pei, Q. B., 2010, "Advances in Dielectric Elastomers for Actuators and Artificial Muscles," Macromol. Rapid Commun., **31**(1), pp. 10–36.
[5] Anderson, I. A., Gisby, T. A., McKay, T. G., O'Brien, B. M., and Calius, E. P., 2012, "Multi-Functional Dielectric Elastomer Artificial Muscles for Soft and Smart Machines," J. Appl. Phys., **112**(4), p. 041101.
[6] Huang, X., Baroudi, A. E., and Wu, B., 2023, "Vibration Properties of an Elastic Gold Nanosphere Submerged in Viscoelastic Fluid," Mod. Phys. Lett. B, **37**(33), p. 2350174.
[7] Wang, X., Mitchell, S. K., Rumley, E. H., Rothemund, P., and Keplinger, C., 2020, "High-Strain Peano-HASEL Actuators," Adv. Funct. Mater., **30**(7), p. 1908821.
[8] Kellaris, N., Venkata, V. G., Smith, G. M., Mitchell, S. K., and Keplinger, C., 2018, "Peano-HASEL Actuators: Muscle-Mimetic, Electrohydraulic Transducers That Linearly Contract on Activation," Sci. Rob., **3**(14), p. eaar3276.
[9] Polygerinos, P., Correll, N., Morin, S. A., Mosadegh, B., Onal, C. D., Petersen, K., Cianchetti, M., Tolley, M. T., and Shepherd, R. F., 2017, "Soft Robotics: Review of Fluid-Driven Intrinsically Soft Devices; Manufacturing, Sensing, Control, and Applications in Human-Robot Interaction," Adv. Eng. Mater., **19**(12), p. 1700016.
[10] Acome, E., Mitchell, S. K., Morrissey, T. G., Emmett, M. B., Benjamin, C., King, M., Radakovitz, M., and Keplinger, C., 2018, "Hydraulically Amplified Self-Healing Electrostatic Actuators With Muscle-Like Performance," Science, **359**(6371), pp. 61–65.
[11] Rothemund, P., Kirkman, S., and Keplinger, C., 2020, "Dynamics of Electrohydraulic Soft Actuators," Proc. Natl. Acad. Sci. U. S. A., **117**(28), pp. 16207–16213.
[12] Rothemund, P., Kellaris, N., Mitchell, S. K., Acome, E., and Keplinger, C., 2021, "HASEL Artificial Muscles for a New Generation of Lifelike Robots—Recent Progress and Future Opportunities," Adv. Mater., **33**(19), p. 2003375.
[13] Yoder, Z., Kellaris, N., Chase-Markopoulou, C., Ricken, D., Mitchell, S. K., Emmett, M. B., Weir, R. F. F., Segil, J., and Keplinger, C., 2020, "Design of a High-Speed Prosthetic Finger Driven by Peano-HASEL Actuators," Front. Robot. AI, **7**, pp. 2296–9144.
[14] Yoder, Z., Macari, D., Kleinwaks, G., Schmidt, I., Acome, E., and Keplinger, C., 2023, "A Soft, Fast and Versatile Electrohydraulic Gripper With Capacitive Object Size Detection," Adv. Funct. Mater., **33**(3), p. 2209080.
[15] Kellaris, N., Rothemund, P., Zeng, Y., Mitchell, S. K., Smith, G. M., Jayaram, K., and Keplinger, C., 2021, "Spider-Inspired Electrohydraulic Actuators for Fast, Soft-Actuated Joints," Adv. Sci., **8**(14), p. 2100916.
[16] Hunt, S., McKay, T. G., and Anderson, I. A., 2014, "A Self-Healing Dielectric Elastomer Actuator," Appl. Phys. Lett., **104**(11), p. 113701.
[17] Pelrine, R. E., Kornbluh, R. D., and Joseph, J. P., 1998, "Electrostriction of Polymer Dielectrics With Compliant Electrodes as a Means of Actuation," Sens. Actuators, A, **64**(1), pp. 77–85.
[18] Baumhauer, J. C., and Tiersten, H. F., 1973, "Nonlinear Electroelastic Equations for Small Fields Superposed on a Bias," J. Acoust. Soc. Am., **54**(4), pp. 1017–1034.
[19] Toupin, R. A., 1956, "The Elastic Dielectric," Arch. Ration. Mech. Anal., **5**(6), pp. 849–915.
[20] Toupin, R. A., 1963, "A Dynamical Theory of Elastic Dielectrics," Int. J. Eng. Sci., **1**(1), pp. 101–126.
[21] Dorfmann, A., and Ogden, R., 2005, "Nonlinear Electroelasticity," Acta Mech., **174**(3–4), p. 167.
[22] McMeeking, R. M., and Landis, C. M., 2005, "Electrostatic Forces and Stored Energy for Deformable Dielectric Materials," ASME J. Appl. Mech., **72**(4), pp. 581–590.
[23] Suo, Z. G., Zhao, X. H., and Greene, W. H., 2008, "A Nonlinear Field Theory of Deformable Dielectrics," J. Mech. Phys. Solids, **56**(2), pp. 467–486.
[24] Shmuel, G., and deBotton, G., 2013, "Axisymmetric Wave Propagation in Finitely Deformed Dielectric Elastomer Tubes," Proc. R. Soc. A: Math. Phys. Eng. Sci., **469**(2155), p. 20130071.
[25] Dorfmann, L., and Ogden, R. W., 2020, "Waves and Vibrations in a Finitely Deformed Electroelastic Circular Cylindrical Tube," Proc. R. Soc. A: Math. Phys. Eng. Sci., **476**(2233), p. 20190701.
[26] Zhu, J., Stoyanov, H., Kofod, G., and Suo, Z. G., 2010, "Large Deformation and Electromechanical Instability of a Dielectric Elastomer Tube Actuator," J. Appl. Phys., **108**, p. 074113.
[27] Melnikov, A., and Ogden, R. W., 2018, "Bifurcation of Finitely Deformed Thick-Walled Electroelastic Cylindrical Tubes Subject to a Radial Electric Field," Z. Angew. Math. Phys., **69**, p. 60.
[28] Dorfmann, L., and Ogden, R. W., 2019, "Instabilities of Soft Dielectrics," Philos. Trans. R. Soc. A: Math. Phys. Eng. Sci., **377**(2144), p. 20180077.
[29] Biot, M. A., 1952, "Propagation of Elastic Waves in a Cylindrical Bore Containing a Fluid," J. Appl. Phys., **23**(9), pp. 997–1005.
[30] Fuller, C. R., and Fahy, F. J., 1982, "Characteristics of Wave Propagation and Energy Distributions in Cylindrical Elastic Shells Filled With Fluid," J. Sound Vib., **81**(4), pp. 501–518.

[31] Chen, W. Q., and Bian, Z. G., 2011, "Wave Propagation in Submerged Functionally Graded Piezoelectric Cylindrical Transducers With Axial Polarization," Mech. Adv. Mater. Struct., **18**(1), pp. 85–93.

[32] Chen, W. Q., Bian, Z. G., Lv, C. F., and Ding, H. J., 2004, "3D Free Vibration Analysis of a Functionally Graded Piezoelectric Hollow Cylinder Filled With Compressible Fluid," Int. J. Solids Struct., **41**(3), pp. 947–964.

[33] Defaz, R. I., Epstein, M., and Federico, S., 2021, "Analysis of Solitary Waves in Fluid-Filled Thin-Walled Electroactive Tubes," Mech. Res. Commun., **113**, p. 103654.

[34] Cao, Y., Wu, B., Carrera, E., Rudykh, S., and Chen, W. Q., 2024, "Axisymmetric Vibration of Multilayered Electroactive Circular Plates in Contact With Fluid," J. Sound Vib., **573**, p. 118189.

[35] Zhao, X., and Suo, Z., 2007, "Method to Analyze Electromechanical Stability of Dielectric Elastomers," Appl. Phys. Lett., **91**(6), p. 061921.

[36] Su, Y. P., Conroy Broderick, H., Chen, W. Q., and Destrade, M., 2018, "Wrinkles in Soft Dielectric Plates," J. Mech. Phys. Solids, **119**, pp. 298–318.

[37] Dorfmann, L., and Ogden, R. W., 2014, *Nonlinear Theory of Electroelastic and Magnetoelastic Interactions*, Springer, New York.

[38] Wu, B., Su, Y. P., Chen, W. Q., and Zhang, C., 2017, "On Guided Circumferential Waves in Soft Electroactive Tubes Under Radially Inhomogeneous Biasing Fields," J. Mech. Phys. Solids, **99**, pp. 116–145.

[39] Weiqiu, C., Ding, H. J., Guo, Y. M., and Yang, Q. D., 1997, "Free Vibrations of Fluid-Filled Orthotropic Cylindrical Shells," J. Eng. Mech., **123**(11), pp. 1130–1133.

[40] Chen, W. Q., Liu, D. Y., Kitipornchai, S., and Yang, J., 2017, "Bifurcation of Pressurized Functionally Graded Elastomeric Hollow Cylinders," Composites, Part B, **109**, pp. 259–276.

[41] Su, Y. P., 2020, "Voltage-Controlled Instability Transitions and Competitions in a Finitely Deformed Dielectric Elastomer Tube," Int. J. Eng. Sci., **157**, p. 103380.

[42] Gent, A. N., 1996, "A New Constitutive Relation for Rubber," Rubber Chem. Technol., **69**(1), pp. 59–61.

[43] Ding, H. J., and Chen, W. Q., 2001, *Three Dimensional Problems of Piezoelasticity*, Nova Science, Huntington, New York.

[44] Pestel, E. C., and Leckie, F. A., 1963, *Matrix Methods in Elastomechanics*, McGraw-Hill, New York.

[45] Wu, B., Destrade, M., and Chen, W. Q., 2020, "Nonlinear Response and Axisymmetric Wave Propagation in Functionally Graded Soft Electro-Active Tubes," Int. J. Mech. Sci., **187**, p. 106006.